JGR Planets

RESEARCH ARTICLE

10.1029/2024JE008331

# Mid-Infrared Reflectance and Emissivity Spectra of High Porosity Regoliths

**Audrey C. Martin[1], Joshua P. Emery[2], Mark Loeffler[2,3], and Kerri L. Donaldson Hanna[1]**

[1]Department of Physics, University of Central Florida, Orlando, FL, USA, [2]Department of Astronomy and Planetary Science, Northern Arizona University, Flagstaff, AZ, USA, [3]Center for Material Interfaces in Research and Applications, Northern Arizona University, Flagstaff, AZ, USA

**Key Points:**

- Regolith porosity, and measurement conditions are important variables that affect the mid-infrared spectra of fine particulate silicates
- Kirchhoff's Law can be reliably applied to high-porosity samples of fine particulate silicates
- Researchers can confidently utilize ambient reflectance spectra for studying airless bodies by considering known environmental spectral effects

**Correspondence to:**

A. C. Martin,
Audrey.Martin@ucf.edu

**Citation:**

Martin, A. C., Emery, J. P., Loeffler, M., & Donaldson Hanna, K. L. (2025). Mid-infrared reflectance and emissivity spectra of high porosity regoliths. *Journal of Geophysical Research: Planets*, *130*, e2024JE008331. https://doi.org/10.1029/2024JE008331

Received 12 FEB 2024
Accepted 18 APR 2025

**Author Contributions:**

**Conceptualization:** Audrey C. Martin, Joshua P. Emery
**Data curation:** Audrey C. Martin
**Formal analysis:** Audrey C. Martin, Joshua P. Emery, Kerri L. Donaldson Hanna
**Funding acquisition:** Audrey C. Martin, Joshua P. Emery
**Investigation:** Joshua P. Emery
**Methodology:** Audrey C. Martin
**Resources:** Joshua P. Emery, Mark Loeffler
**Supervision:** Joshua P. Emery, Mark Loeffler, Kerri L. Donaldson Hanna
**Writing – original draft:** Audrey C. Martin
**Writing – review & editing:** Audrey C. Martin, Joshua P. Emery, Mark Loeffler, Kerri L. Donaldson Hanna



**Abstract** Mid-infrared (MIR; 5–35 μm) spectroscopy is often used for mineralogical identification on planetary surfaces. Laboratory spectra aiding remote sensing observations are typically performed in reflection geometries, while MIR spectra of planetary surfaces are typically obtained via emission. Here we explore the validity of Kirchhoff's Law in converting reflectance to emissivity spectra, focusing on the high-porosity regoliths found on airless bodies such as the Moon and asteroids. Specifically, we compared ambient reflectance, ambient emissivity, and simulated asteroid environment (SAE) spectra of fine-particulate olivine and pyroxene with varying regolith porosities, focusing on how spectral features, including the Christiansen feature (CF), reststrahlen bands (RBs), and transparency features (TF), changed under these different conditions. Our results indicate that Kirchhoff's Law can be effectively employed to interpret 19 MIR reflectance spectra of high-porosity samples, provided environmental spectral effects (i.e., spectral changes due to different pressure and temperature conditions) are considered.

**Plain Language Summary** This study explores the use of mid-infrared spectroscopy to understand planetary surfaces, focusing on high porosity regoliths as found on the Moon and some asteroids. The research tests the validity of Kirchhoff's Law for high porosity regoliths by measuring fine-particulate silicates in three ways: ambient reflectance, ambient emissivity, and simulated asteroid environment (SAE). The findings suggest that Kirchhoff's Law can be reliably applied to high-porosity samples. Kirchhoff's Law states that hemispherical reflectance (R) and emissivity (E) spectra are related via the following equation: E = 1-R. The study emphasizes the need to consider environmental effects (i.e., spectral changes due to different pressure and temperature conditions) when using ambient laboratory spectra for airless body studies. Regolith porosity, and measurement conditions are important variables that affect the mid-infrared spectra of fine particulate silicates. Kirchhoff's Law can be reliably applied to high-porosity samples of fine particulate silicates.

## 1. Introduction

Mid-infrared (MIR; 5–35 μm) spectroscopy is a useful tool for understanding planetary surfaces. Because the MIR wavelength region is sensitive to a variety of entwined variables, it is necessary to parse through individual effects in a controlled laboratory setting for robust and accurate interpretations of spectra obtained from distant object surfaces. Parameters such as composition, particle size fraction, regolith porosity, and environmental conditions all affect the position, depth, and shape of mineralogically identifiable bands frequently used in remote sensing studies (e.g., Donaldson Hanna et al., 2017; Martin et al., 2022, 2023; Mustard & Hays, 1997; Salisbury & Wald, 1992).

Most spectral libraries are measured in reflectance (e.g., Reflectance Experiment LABoratory (RELAB) and Advanced Spaceborne Thermal Emission and Reflectance Radiometer (ASTER) spectral libraries) and used for comparison to remote sensing emissivity spectra (e.g., Martin et al., 2022, 2023; Takir et al., 2015; Vernazza et al., 2012). A notable exception is Arizona State University's emissivity spectral library (speclib.asu.edu) which is widely used in terrestrial and Martian spectral studies. As is typical in the planetary sciences, many researchers invoke Kirchhoff's Law (E = 1-R) to convert from reflectance to emissivity space. Though Kirchhoff's Law is strictly valid for hemispherical reflectance, and for materials in thermodynamic equilibrium, this approach has been shown to work well for samples with low regolith porosity (e.g., Bramble et al., 2021a, 2021b; Maturilli et al., 2015, 2016; Salisbury et al., 1991, 1994; Young et al., 2019), however, this has not been verified for high regolith porosity samples. Given that an increasing number of planetary surfaces are being measured in the MIR and that many of these surfaces have highly porous regoliths, it is critical to test the validity of Kirchhoff's Law in higher porosity materials.

Besides testing the validity of converting reflectance spectra to emissivity in higher porosity materials, it is also important to fully characterize how environmental conditions affect the MIR spectra of these materials. Studies with low-porosity samples (<60% void space) have shown that MIR emissivity spectra are highly sensitive to the sample's brightness temperature, the temperature gradient within the upper hundreds of microns of the sample, and the atmospheric pressure of the chamber in which they are measured (e.g., Donaldson Hanna et al., 2017; Logan & Hunt, 1970; Maturilli et al., 2016; Shirley et al., 2023; Shirley & Glotch, 2019). The observed MIR spectral effects owing to the vacuum environment are due to thermal gradients in the near-surface (upper 100 μm) and a material's wavelength-dependent scattering properties (e.g., Henderson & Jakosky, 1997). The intensity and shape of a thermal gradient are dependent on factors including albedo, brightness temperature, particle size fraction, and regolith porosity—which in turn affect the contrast and shape of important spectral features used for compositional identification. These spectral effects are caused, in part, by photons emitting from deeper hotter regions within the subsurface that are more transparent at shorter wavelengths (<8 μm; Donaldson Hanna et al., 2012, 2019; Hapke, 1996). As such, we also aim to study environmental effects for high porosity samples (≳60% void space) taken in emissivity space, which are relevant for the Moon and many asteroid surfaces.

This work is one of a series that investigates how regolith porosity affects the MIR spectra of astrophysically relevant minerals. Our previous studies show that regolith porosity greatly affects the MIR spectral features of fine particulate (<63 μm) olivine and pyroxene samples (Martin et al., 2022, 2023). We took those previous measurements under ambient conditions in reflectance space. Now, we compare select reflectance spectra of fine-particulate olivine and pyroxene samples with high regolith porosity to emissivity spectra of the same samples taken in both ambient and simulated asteroid environment (SAE) conditions with the goal of answering the question: *To what degree can ambient reflectance spectra of high porosity material be used to interpret remote sensing spectra?* Specifically, we identify mineralogically characteristic features within each MIR spectrum and compare each feature's position and spectral contrast under the different environmental conditions.

## 2. Methods

### 2.1. Sample Suite and Preparation

In this study, we used forsteritic olivine ($Fo_{91}$) and hedenbergite pyroxene ($Wo_{57}En_3Fs_{40}$) samples purchased from the Mineralogical Research Company. As both samples are natural, we identified trace minerals via Electron Microprobe (EMP) analysis. For full mineralogical analyses of each sample, see Martin et al. (2022; $OLV_1$) and Martin et al. (2023; $HEN_1$).

We ground and dry-sieved the silicates into the 45–63 μm particle size fraction using a Gilson Performer III Sieve Shaker. We also sieved the olivine samples into the <20 μm particle size fraction. We then mixed potassium bromide (KBr), ground and sieved into the same particle size fractions, with each silicate acting as a proxy for regolith porosity as it is transparent in the MIR (e.g., Izawa et al., 2021; Martin et al., 2022, 2023; Vernazza et al., 2012). We mixed the silicate powders with KBr in ratios from 0% to 90% by weight in 10 wt% intervals. Sample mixtures and endmember powders were stored in desiccant cabinets to minimize atmospheric water adsorption. When filling the sample cups, we aimed to not compress the sample in any way (e.g., via tapping). We leveled the sample cup surface with a razor blade at approximately 45° to fill the cup completely and avoid compaction.

It is important to note that KBr is a good proxy for regolith porosity when considering its optical properties, but there are some caveats. First, in this paper we use the term "regolith porosity" to strictly mean "weight percent KBr" as it is consistent with previous studies (e.g., Izawa et al., 2021; King et al., 2011; Martin et al., 2022, 2023). There is additional empty space (or "void space") within the sample that adds to the overall porosity we call "sample cup porosity". Adding the volume percent of KBr to the sample cup porosity, we get the "total optical porosity'—which is the total volume of space within a sample cup that accounts for the optical porosity (Table 1). Additional information on this value can be found in Martin et al. (2022) Section 2.2 (Note that "total *optical* porosity" in this paper is called "total *simulated* porosity" in Martin et al.). The second caveat to note for using KBr is that it is not a robust *thermophysical* proxy for porosity. Though KBr allows for photons emitted from silicates to pass through relatively unobstructed areas, it conducts and radiates heat—while empty space does not. KBr's thermal conductivity plays an important role in establishing a thermal gradient in vacuum measurements (more discussion on this in Section 5.3). Nonetheless, to understand the optical properties of high regolith porosity samples, we are constrained to the use of KBr regardless of its thermophysical nature.

**Table 1**
*The Weight Percent of KBr in a Sample (Regolith Porosity Rounded to the Nearest 10%), the Percent Volumetric Contribution of Void Space in a Sample Cup (Sample Cup Porosity), and the Combined Percent Volumetric Contribution of Void Space and KBr in a Sample Cup (Total Optical Porosity) Is Listed for Each Sample*

| Sample | Regolith porosity (wt.% KBr) | Sample cup porosity (vol.% void) | Total optical porosity (vol.% void + KBr) |
|---|---|---|---|
| Olivine (45–63 μm) | 0.00 | 61.12 | 61.12 |
| | 10.00 | 61.11 | 65.65 |
| | 30.00 | 61.47 | 74.48 |
| | 50.00 | 56.75 | 80.24 |
| | 90.00 | 57.47 | 96.36 |
| Olivine (<20 μm) | 0.00 | n.m.[a] | ~72.65[a] |
| | 10.00 | 71.22 | 74.58 |
| | 50.00 | 72.18 | 87.29 |
| | 90.00 | 74.56 | 97.82 |
| Pyroxene (45–63 μm) | 0.00 | 61.23 | 61.23 |
| | 30.35 | 58.30 | 73.31 |
| | 49.75 | 56.83 | 81.05 |
| | 69.05 | 55.00 | 88.40 |

[a]No measurement (n.m.) of the sample cup porosity was made for olivine (<20 μm) 0% regolith porosity sample—the listed total optical porosity is an average of the other olivine (<20 μm) sample cup porosity measurements.

### 2.2. Measurement

We measured all reflectance spectra using a Thermo-Nicolet iS50 Fourier Transform infrared (FTIR) spectrometer under ambient conditions (Martin et al., 2022, 2023). We measured the reflected intensity of our sample using a PIKE Technologies EasiDiff diffuse reflectance accessory, averaging 200 scans between 4,000 and 4,400 $cm^{-1}$ (2.5–25 μm) at 4 $cm^{-1}$ resolution. We measured each sample two or more times after rotating the sample cup ~90° and averaged them to get the average reflected intensity ($I_s$), taking the standard deviation of the measurements as the error. We measured the reflected intensity of pure KBr powder with the same particle size distribution as the target silicate mixture in the reference spectrum ($I_{ref}$). Finally, using Kirchhoff's Law, we converted reflectance ($R = I_s/I_{ref}$) to emissivity ($E$ = 1-R). We note that Kirchhoff's Law is strictly valid for hemispherical reflectance, but in practice diffuse reflectance does not significantly affect band positions, shapes, or relative strengths (Salisbury et al., 1991, 1994), and here we compare the diffuse reflectance spectra to emissivity spectra.

We made emissivity measurements of the following sample mixtures (listed as wt.% KBr—similarly referred to as "regolith porosity"): Olivine (45–63 μm) 0%, 10%, 30%, 50%, and 90%, olivine (<20 μm) 0%, 10%, 50%, and 90%, and pyroxene (45–63 μm) 0%, 30%, 50%, and 70%. We made all our emissivity measurements using the Planetary Analogue Surface Chamber for Asteroid and Lunar Environments (PASCALE) attached to a Bruker VERTEX 70v FTIR spectrometer at the University of Central Florida. To obtain a spectrum, we took 250 scans between 2,000 and 400 $cm^{-1}$ (5–25 μm) with 4 $cm^{-1}$ spectral resolution in ambient and simulated asteroid environment (SAE) conditions calibrated to measurements of a blackbody target (e.g., Donaldson Hanna et al., 2017, 2021). We omit the region around ~16 μm due to the low signal throughput of the Bruker Wide Range beamsplitter. To achieve ambient conditions, we backfilled the chamber with ~1,000 mbar of dry $N_2$, held the chamber at ambient temperature, and heated the sample holder from below to 353 K. For SAE measurements, we evacuated chamber to $<1 \times 10^{-4}$ mbar, cooled the chamber to <125 K as measured by temperature sensors in the internal radiation shield and the dewar, heated the sample holder from below to 333 K, and used a solar-like halogen lamp to produce a surface brightness temperature of 350 K. We estimate the surface brightness temperature by fitting a plank function to the measured emitted signal (see Donaldson Hanna et al., 2021 for detailed schematics of PASCALE). These temperature and pressure conditions create thermal gradients within the sample consistent with those expected within the regolith found on the surfaces of airless bodies such as the Moon (at lunar noon for high latitudes) and highly reflective asteroids such as S-types (e.g., Herganrother et al., 2014; Williams et al., 2017). We calculated emissivity and uncertainties using the methods outlined by Donaldson Hanna et al. (2021).

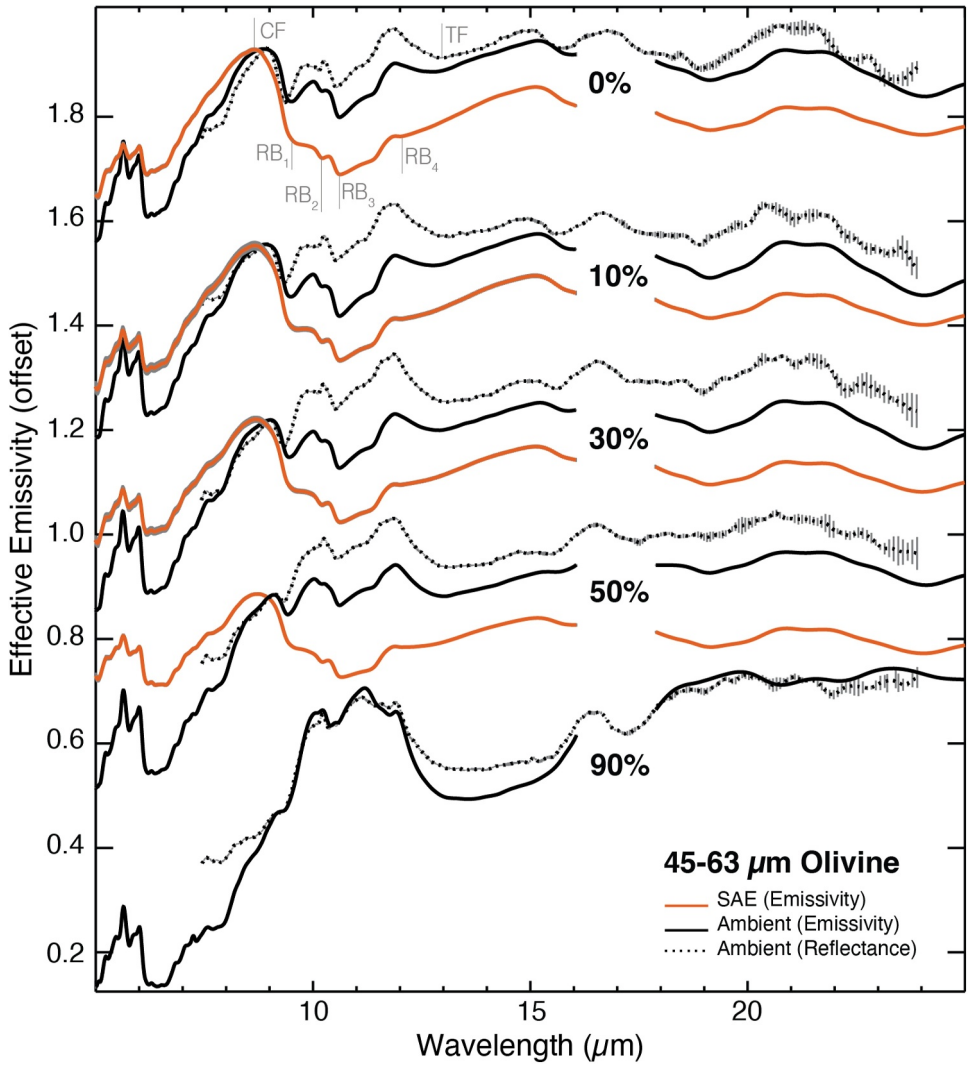


**Figure 1.** Reflectance and emissivity spectra of particulate olivine mixed with increasing wt% of KBr from top to bottom to represent regolith porosity (i.e., 0% regolith porosity spectra on top, and 90% regolith porosity on bottom) of 45–63 μm sized particles. The orange solid line spectra were taken in SAE, while the black solid and dashed line spectra were taken in ambient environment. Spectra of the same samples are vertically shifted to have the same effective emissivity at the CF for clarity and ease of comparison. The CF and RBs are labeled on each 0% regolith porosity SAE spectrum. The TF is labeled on the 0% regolith porosity reflectance spectrum. Measurement error is shown with gray bars (more apparent in reflectance spectra at long wavelengths, and emissivity spectra at short wavelengths). Note that emissivity spectra around 16 μm is omitted due to low signal and are not included in analysis.

## 3. Results

We show average reflectance and emissivity measurements of 45–63 μm olivine, <20 μm olivine, and 45–63 μm pyroxene powders in Figures 1–3. Note that we were unable to take SAE spectra of the 90% regolith porosity olivine samples because their high albedo does not allow the samples to be heated to the necessary brightness temperature and hold that temperature consistently for the duration of a measurement run (~20 min). Regardless, to characterize how spectra taken under different conditions change, we identified the Christiansen feature (CF; a feature caused by a transition in a strong band between volume and surface scattering along the electromagnetic spectrum), reststrahlen bands (RBs; wavelength dependent regions of increased reflectance), and transparency features (TF; spectral regions of low absorption). Spectral analysis descriptions are detailed in Section 4.

The reflectance and ambient emissivity spectra of 0% regolith porosity samples of olivine (45–63 μm) closely resemble each other (Figure 1). In contrast, the 0% regolith porosity SAE spectrum displays a more prominent CF

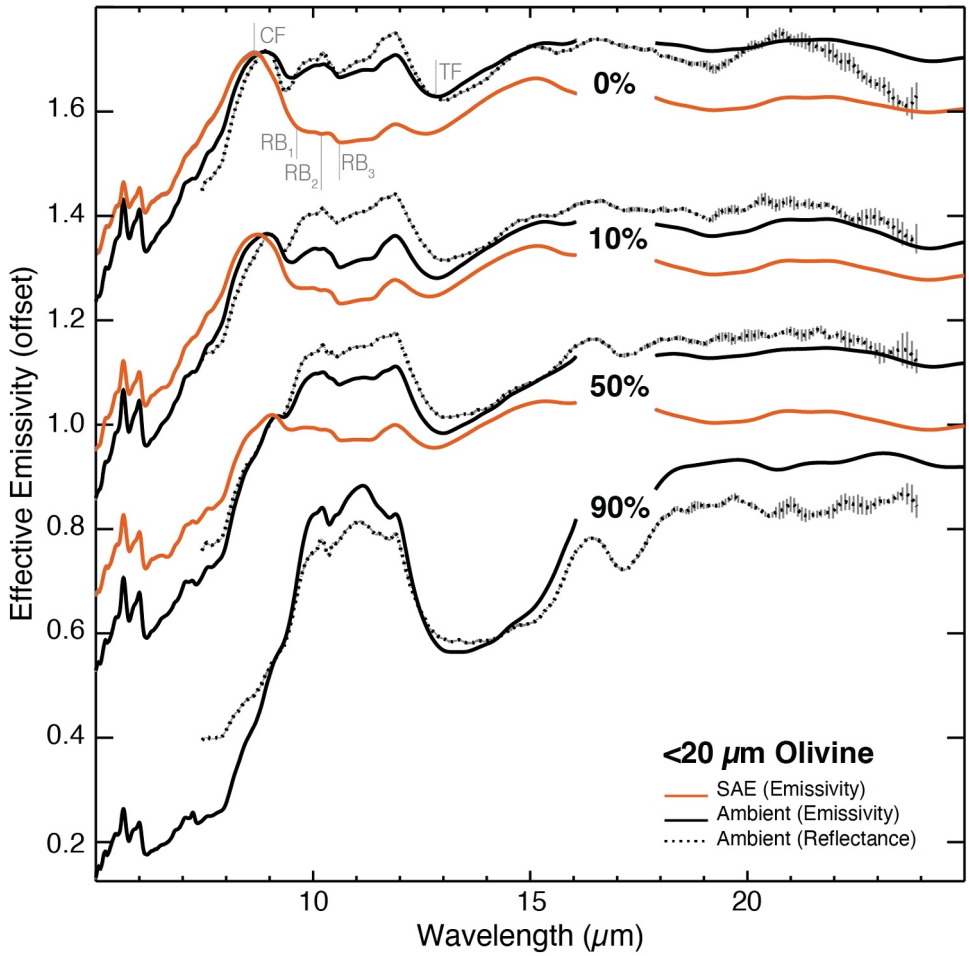


**Figure 2.** Reflectance and emissivity spectra of particulate olivine mixed with increasing wt% of KBr from top to bottom to represent regolith porosity (i.e., 0% regolith porosity spectra on top, and 90% regolith porosity on bottom) of <20 μm sized particles. The orange solid line spectra were taken in SAE, while the black solid and dashed line spectra were taken in ambient environment. Spectra of the same samples are vertically shifted to have the same effective emissivity at the CF for clarity and ease of comparison. The CF and RBs are labeled on each 0% regolith porosity SAE spectrum. The TF is labeled on the 0% regolith porosity reflectance spectrum. Measurement error is shown with gray bars (more apparent in reflectance spectra at long wavelengths, and emissivity spectra at short wavelengths). Note that emissivity spectra around 16 μm is omitted due to low signal and are not included in analysis.

(~8.6 μm) and the presence of $RB_4$ (~12.1 μm). As regolith porosity increases, both the reflectance and ambient emissivity spectra show smaller (e.g., less wide and lower effective emissivity values) CFs (~8.9 μm) and deeper TFs (~12.8 μm), while the SAE spectra remain relatively unchanged. Both 90% regolith porosity spectra of olivine (45–63 μm) taken under ambient conditions show a prominent 10-μm plateau and wide TF. The 10-μm plateau is a feature common in comet and primitive asteroid spectra consisting of somewhat muted silicate bands from ~9.5 to 13 μm (e.g., Kelley et al., 2017; Martin & Emery, 2023).

Like the olivine (45–63 μm) spectra, the reflectance and ambient emissivity spectra of 0% regolith porosity samples of olivine (<20 μm) resemble each other, while the SAE spectrum exhibits a pronounced CF (~8.9 μm; Figure 2). Unlike the SAE olivine (45–63 μm) spectra, the SAE olivine (<20 μm) spectra lack an $RB_4$ and the SAE spectra undergo changes with increasing regolith porosity. The SAE CF diminishes, and the RBs become shallower, mirroring the trend observed in reflectance and ambient emissivity spectra. The 90% regolith porosity spectra of olivine (<20 μm) spectra taken under ambient conditions show a prominent 10-μm plateau and deep TF.

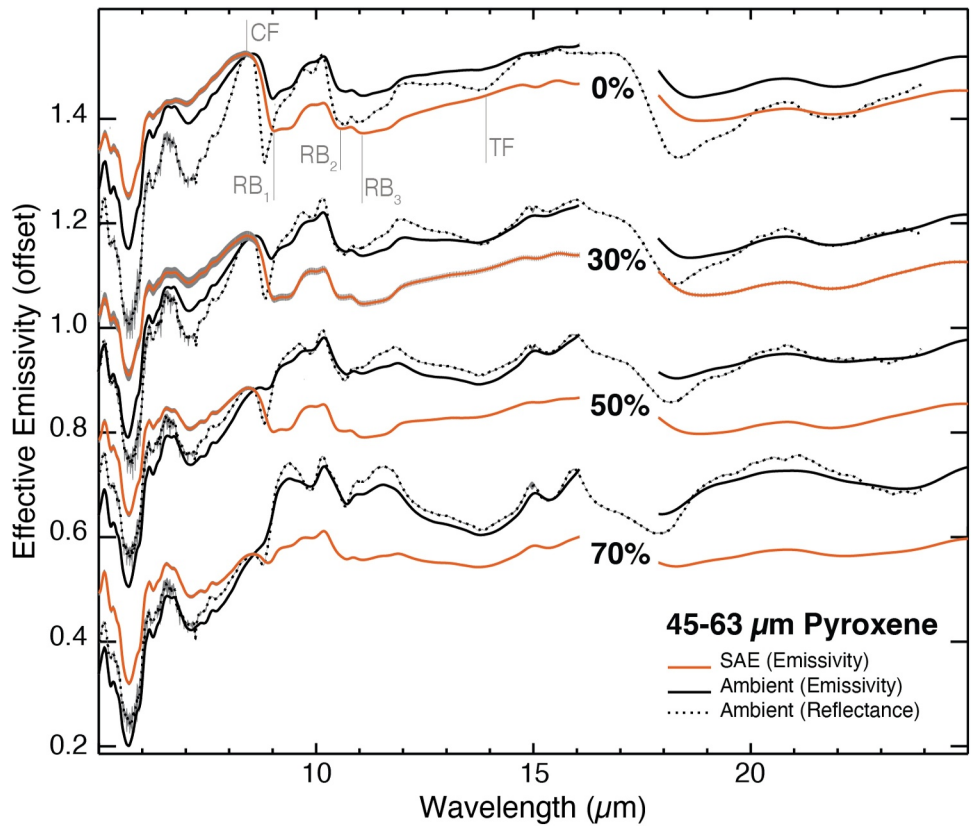


**Figure 3.** Reflectance and emissivity spectra of particulate pyroxene mixed with increasing wt% of KBr from top to bottom to represent regolith porosity (i.e., 0% regolith porosity spectra on top, and 70% regolith porosity on bottom). The orange solid line spectra were taken in SAE, while the black solid and dashed line spectra were taken in ambient environment. Spectra of the same samples are vertically shifted to have the same effective emissivity at the CF for clarity and ease of comparison. The CF and RBs are labeled on each 0% regolith porosity SAE spectrum. The TF is labeled on the 0% regolith porosity reflectance spectrum. Measurement error is shown with gray bars. Note that emissivity spectra around 16 μm is omitted due to low signal and are not included in analysis.

Unlike the 0% regolith porosity of olivine, we observed differences in the reflectance and ambient emissivity spectra of 0% regolith porosity samples of pyroxene (Figure 3). Specifically, the SAE and ambient emissivity spectra share similar CF shapes (~8.4 μm), have a box-like shaped $RB_1$ (~9.0 μm), and shallow $RB_2$ (~10.6 μm), $RB_3$ (~11.1 μm), and TF (~13.8 μm), whereas the reflectance spectrum has a sharp $RB_1$ (~8.8 μm) and more defined TF (~13.7 μm). As regolith porosities increase, the reflectance and ambient emissivity spectra begin to look more similar, whereas the SAE spectra of 0%, 30%, and 50% regolith porosity samples show minimal change. Like the 90% regolith porosity spectra of olivine taken under ambient conditions, the 70% regolith porosity reflectance and ambient emissivity spectra of pyroxene has a defined 10-μm plateau and deep TF, while the SAE spectrum lacks these characteristics.

## 4. Spectral Analysis

As mentioned in the previous section, we identified the CF, RBs, and the TF in each spectrum. We label the positions of these features in Figures 1–3 and quantify how their position changes with regolith porosity in Figure 4. We chose these features for analysis because they are widely used in remote sensing/planetary science for identifying mineralogy (e.g., Donaldson Hanna et al., 2021; Hamilton et al., 2021; Kelley et al., 2017; Kumari et al., 2024; Martin & Emery, 2023). We additionally analyzed the spectral contrast of these features, as Martin et al. (2022, 2023) found that the spectral contrast of individual features is dependent on regolith porosity. We calculated the position, spectral contrast, and associated error of these features using the method outlined in Martin et al. (2022) and briefly below.

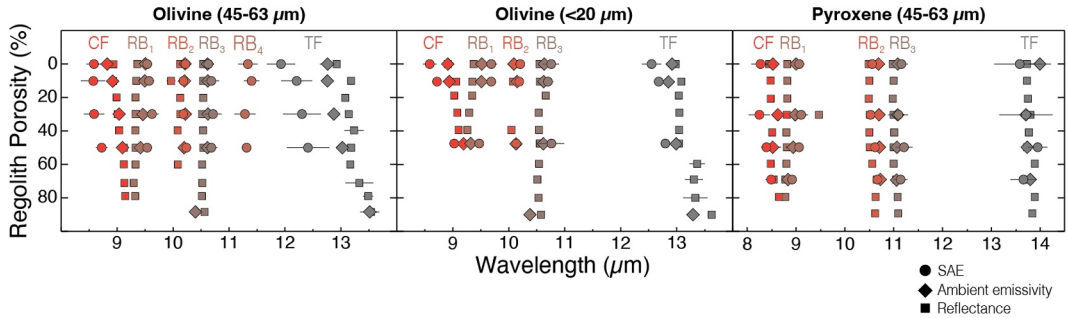


**Figure 4.** The positions of CFs, RBs, and TFs as a function of regolith porosity for spectra of olivine (45–63 μm), olivine (<20 μm), and pyroxene (45–63 μm). Circle, diamond, and square symbols denote SAE, ambient emissivity, and reflectance measurements respectively. Different shades of red/gray are used to distinguish individual features within a plot.

### 4.1. Feature Parameterization Error

We identified and parameterized the CF, TF, and RBs in all spectra using a feature-finding routine originally built and detailed in Martin et al. (2022). In addition to identifying feature position and spectral contrast, the benefit of using this routine is the estimation of the associated error in each of these parameters. First, the feature is located on a Gaussian smoothed spectral segment. After extracting an individual feature from the spectrum, we generated 10,000 "synthetic" versions of that feature by assigning random values within the bounds of the error bar at each wavelength. Then, we use a convex hull approach to determine the upper and lower position bounds of the synthetic feature. We then fit the synthetic feature with a 4th order spline polynomial and calculate the feature's position and spectral contrast. Here we define spectral contrast as the height of the feature above the feature continuum. We use the mean and standard deviation values of the 10,000 synthetic features as the parameter value and error. We use 10,000 versions to ensure a normal distribution across the parameter space. A detailed description of this routine can be found in Section 4.1.1. by Martin et al. (2022).

### 4.2. Christiansen Feature

The position of the 0% regolith porosity olivine CF measured in ambient reflectance and ambient emissivity are very similar (~8.9 μm in spectra of both particle size fractions; Table 2), as is the 0% regolith porosity pyroxene CF measured in ambient reflectance and ambient emissivity (~8.5 μm; Table 3). As regolith porosity increases to ~50%, the CF shifts toward slightly longer wavelengths in all spectral suites (Figure 4).

The positions of SAE CFs in all reported spectra are at similar but consistently shorter wavelengths compared to both sets of spectra taken under ambient conditions (Figure 4; Tables 1 and 2). For instance, the position offset between SAE and ambient emissivity spectra of 0% regolith porosity spectra is ~0.24 μm for 45–63 μm olivine samples, ~0.31 μm for <20 μm olivine samples and ~0.25 μm for pyroxene (Tables 2 and 3). These position offset values are consistent with similar studies that found offsets between 0.14 and 0.64 μm for olivine and between 0.22 and 0.25 μm for pyroxene (e.g., Bramble et al., 2021a; Donaldson Hanna et al., 2021; Shirley & Glotch, 2019). As the regolith porosity increases, the olivine (45–63 μm) spectra show a consistent offset in position between CFs measured in SAE and both sets of spectra taken under ambient conditions, while the offset in the pyroxene and olivine (<20 μm) spectra decrease as regolith porosity increases. Nonetheless, as described above, the CF position measured in ambient reflectance and emissivity is roughly the same; the position offset between CFs measured in SAE and ambient *emissivity* is similar to is the position offset between CFs measured in SAE and ambient *reflectance* (Figure 4; Tables 1 and 2).

For all three measurement techniques, the spectral contrast of the CF decreases rapidly with increasing regolith porosity (Figures 5–7). The CF is completely gone in all spectra over ~50% regolith porosity except in the SAE and ambient reflectance spectra of pyroxene. Interestingly, we find that the CF spectral contrast in spectra of olivine (<20 μm) decreases more rapidly with increasing regolith porosity than the spectra of the 45–63 μm samples (both olivine and pyroxene) in all measurement conditions, suggesting that the rate of decrease in spectral contrast is more extreme for smaller particles.

**Table 2**
*Olivine Feature Positions of 0% Regolith Porosity Spectra Compared to Positions of Olivine Features Reported in Lane et al. (2011), Hamilton (2010), Shirley and Glotch (2019), and Donaldson Hanna et al. (2021)*

| Spectrum | CF | $RB_1$ | $RB_2$ | $RB_3$ | $RB_4$ | TF |
|---|---|---|---|---|---|---|
| $OLV_{63,ambi}$ | 8.82 ± 0.07 | 9.51 ± 0.01 | 10.21 ± 0.01 | 10.61 ± 0.03 | N/A | 12.76 ± 0.13 |
| $OLV_{63,SAE}$ | 8.58 ± 0.13 | 9.63 ± 0.10 | 10.22 ± 0.02 | 10.63 ± 0.05 | 12.10 ± 0.09 | 11.93 ± 0.25 |
| $OLV_{63,r}$ | 8.94 ± 0.02 | 9.36 ± 0.01 | 10.13 ± 0.01 | 10.54 ± 0.01 | N/A | 12.92 ± 0.05 |
| $OLV_{20,ambi}$ | 8.90 ± 0.08 | 9.52 ± 0.03 | 10.09 ± 0.02 | 10.64 ± 0.07 | N/A | 12.92 ± 0.11 |
| $OLV_{20,SAE}$ | 8.59 ± 0.12 | 9.77 ± 0.11 | 10.20 ± 0.01 | 10.75 ± 0.15 | N/A | 12.55 ± 0.17 |
| $OLV_{20,r}$ | 8.91 ± 0.02 | 9.37 ± 0.01 | 10.11 ± 0.01 | 10.55 ± 0.02 | N/A | 12.98 ± 0.04 |
| $L_e$ | N/A | 9.70 | 10.20 | 11.11* | $12.02^{\bowtie}$ | N/A |
| $L_r$ | N/A | 9.48 | 10.18 | 10.81* | $11.96^{\bowtie}$ | N/A |
| $H_e$ | 8.95 | 9.57 | 10.18 | 10.63 | 11.95 | N/A |
| $H_r$ | 8.79–8.90 | 9.34–9.51 | 10.12–10.16 | 10.51–10.58 | 11.92–11.95 | N/A |
| $S_{32,ambi}$ | 8.90 | 9.48 | N/A | N/A | N/A | 12.96 |
| $S_{32,SAE}$ | 8.76 | 9.48 | N/A | N/A | N/A | 12.96 |
| $S_{63,ambi}$ | 8.87 | 9.48 | N/A | N/A | N/A | 12.96 |
| $S_{63,SAE}$ | 8.69 | 9.48 | N/A | N/A | N/A | 12.96 |
| $D_{ambi}$ | 8.94 | 9.46 | 10.21 | 10.63 | N/A | 12.87 |
| $D_{SAE}$ | 8.83 | 9.69 | 10.21 | 10.63 | N/A | 12.87 |

*Note.* Reflectance and emissivity feature positions of olivine ($Fo_{89.5}$) from Lane et al. (2011) are labeled $L_r$ and $L_e$, respectively. Reflectance and emissivity feature positions of forsterite ($Fo_{90–92}$) from Hamilton (2010) are labeled $H_r$ and $H_e$, respectively. Emissivity measurements taken in ambient and SAE of <32 μm and 32–63 μm olivine ($Fo_{88}$) from Shirley and Glotch (2019) are labeled $S_{32,ambi}$, $S_{32,SAE}$, $S_{63,ambi}$, and $S_{63,SAE}$, respectively. Emissivity measurements taken in ambient and SAE of olivine ($Fo_{91}$) from Donaldson Hanna et al. (2021) are labeled $D_{ambi}$, and $D_{SAE}$, respectively. * and $^{\bowtie}$ Indicate bands labeled "4" and "5" respectively in Lane et al. (2011). Otherwise, band numbers given here correspond to band numbers in comparison papers.

The shape of the CF (as measured from ~7.5 to 10 μm) also depends on the measurement technique. This dependency likely stems from the induced thermal gradient in SAE spectra that changes the temperature and differential heating in the sample with depth. Ambient emissivity CFs are wider compared to the reflectance CFs in all cases besides olivine (45–63 μm) spectra with >10% regolith porosity. Furthermore, SAE CFs are wider than CFs in both ambient spectral suites. The highest emissivity value in SAE spectra is the CF (besides 50% regolith porosity olivine (<20 μm) and 70% regolith porosity pyroxene spectra), whereas the highest emissivity value in

**Table 3**
*Pyroxene Feature Positions of 0% Regolith Porosity Spectra Compared to Positions of Pyroxene Feature of NMNH-R11524 in Hamilton (2000), a 32–63 μm Particle Size Fraction Augite in Shirley and Glotch (2019), and a 0–90 mm Particle Size Fraction Augite in Donaldson Hanna et al. (2021)*

| Spectrum | CF | $RB_1$ | $RB_2$ | $RB_3$ | TF |
|---|---|---|---|---|---|
| $PYX_{ambi}$ | 8.53 ± 0.07 | 9.00 ± 0.02 | 10.69 ± 0.01 | 11.09 ± 0.12 | 14.00 ± 0.23 |
| $PYX_{,SAE}$ | 8.27 ± 0.19 | 9.06 ± 0.11 | 10.56 ± 0.05 | 11.16 ± 0.13 | 13.58 ± 0.52 |
| $PYX_{,r}$ | 8.45 ± 0.02 | 8.82 ± 0.01 | 10.49 ± 0.01 | 10.98 ± 0.01 | 13.73 ± 0.02 |
| $H_e$ | N/A | 9.17 | 10.49 | 11.29 | N/A |
| $S_{ambi}$ | 8.44 | 8.95 | N/A | N/A | 13.54 |
| $S_{SAE}$ | 8.19 | 8.95 | N/A | N/A | 13.54 |
| $D_{ambi}$ | 8.50 | 9.10 | 10.56 | N/A | N/A |
| $D_{SAE}$ | 8.28 | 9.29 | 10.44 | N/A | N/A |

*Note.* See Table 2 for description of nomenclature.

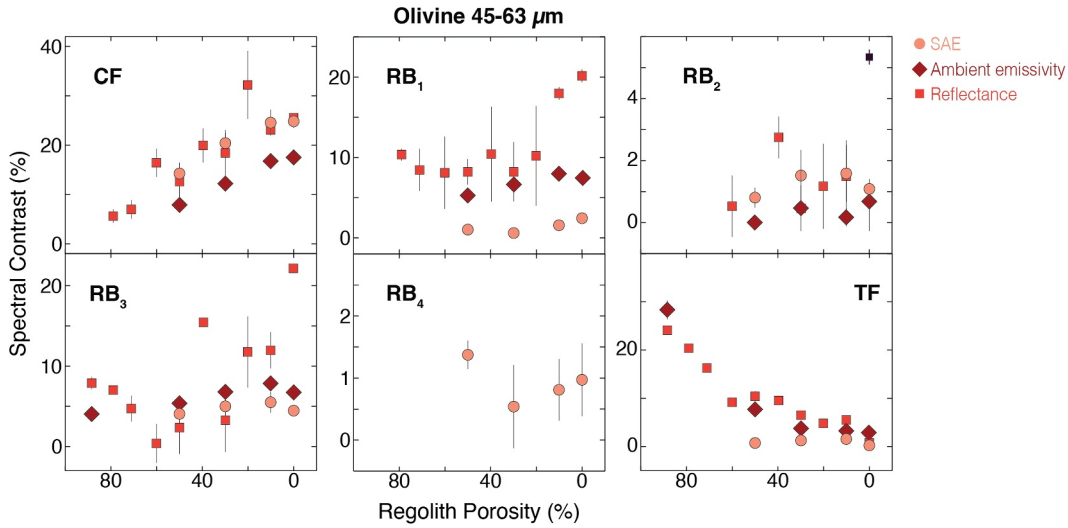


**Figure 5.** Spectral contrast of olivine (45–63 μm) features as a function of regolith porosity. Circle, diamond, and square symbols in different shades of red denote SAE, ambient emissivity, and reflectance measurements, respectively.

converted reflectance spectra tends to be a peak around 12 μm. The CF has the highest emissivity value in ambient emissivity spectra of all 0% and 10% regolith porosity samples, but at higher regolith porosities the ~12 μm peak has the highest emissivity value.

### 4.3. Reststrahlen Bands

As with the CF positions, RBs show very little difference in position between ambient emissivity and reflectance measurements for the 0% regolith porosity samples except for $RB_1$ (Figure 4). As regolith porosity increases, the position offset between reflectance and ambient emissivity feature positions stays roughly the same (~0.15, 0.08, and 0.07 μm for olivine (45–63 μm) $RB_1$, $RB_2$, and $RB_3$, respectively; Table 2). These offsets are consistent with Hamilton (2010) who found offsets in reflectance and emissivity spectra of olivine powder of 0.06–0.23 ($RB_1$) 0.02–0.04 ($RB_2$), and 0.05–0.12 μm ($RB_3$), while Lane et al. (2011) found offsets of ~0.22 ($RB_1$), 0.02 ($RB_2$), and

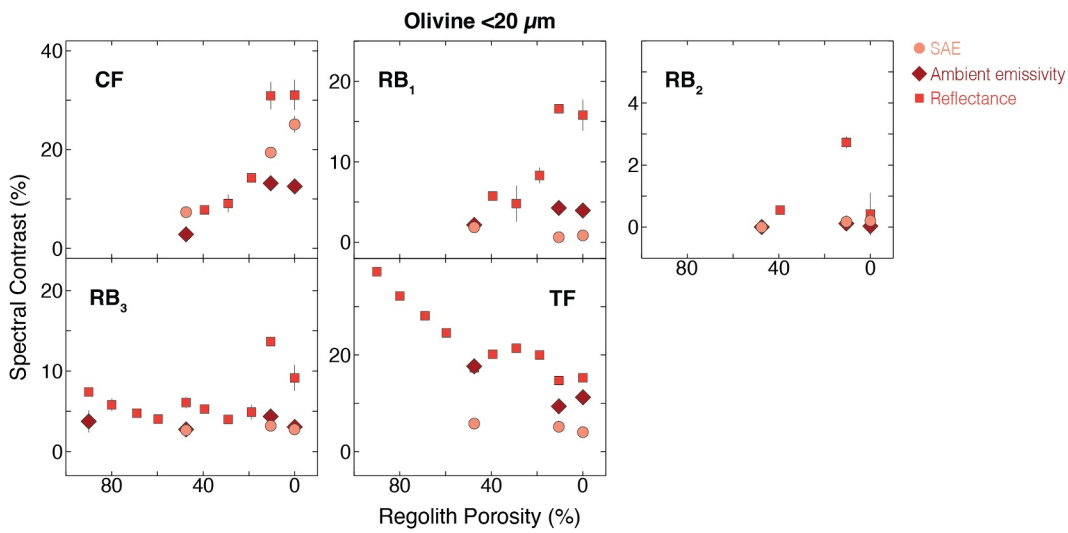


**Figure 6.** Spectral contract of olivine (<20 μm) features as a function of regolith porosity. Circle, diamond, and square symbols in different shades of red denote SAE, ambient emissivity, and reflectance measurements, respectively.

0.30 μm ($RB_3$; Table 2). We note that the RB position offsets are smaller than the CF position offsets, which is

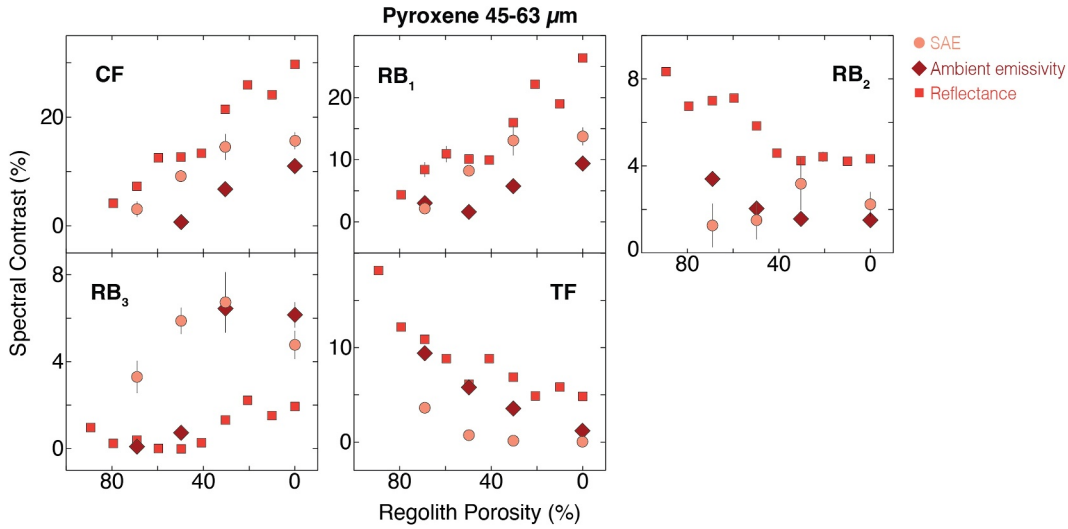


**Figure 7.** Spectral contract of pyroxene (45–63 μm) features as a function of regolith porosity. Circle, diamond, and square symbols in different shades of red denote SAE, ambient emissivity, and reflectance measurements, respectively.

consistent with the results in Bramble et al. (2021a). The smaller offset values are likely due to RBs being caused by molecular absorptions within the crystalline lattice as opposed to the CFs being caused by multiple nuanced optical properties (including the thermal gradient).

In nearly all pyroxene spectra, the RB positions measured in ambient reflectance are at slightly shorter wavelengths than ambient emissivity measurements (~0.18, 0.20, and 0.11 μm for $RB_1$, $RB_2$, and $RB_3$, respectively; Table 3). While few previous studies measured the same pyroxene sample in both reflectance and emissivity, Hamilton (2000) measured the *emissivity* spectra of pyroxene, and the closest analog to our pyroxene (NMNH-R11524). However, the positions of the RBs are not exactly the same as in our ambient emissivity or SAE, which is likely due to the difference in composition.

The relative intensities (i.e., the difference in emissivity values) of the ambient reflectance and emissivity RBs are very similar to each other, whereas the relative intensities of the SAE RBs are distinct. For example, the emissivity values of $RB_1$ and $RB_3$ in olivine (<20 μm) ambient reflectance and emissivity spectra are roughly the same, whereas the SAE emissivity value of $RB_1$ is higher than $RB_3$ (Figure 2). Additionally, in the 30% and 50% regolith porosity spectra of pyroxene, the CF, $RB_2$, and $RB_3$ emissivity values in ambient reflectance and emissivity all align, whereas the SAE $RB_2$ and $RB_3$ are lower relative to the CF (Figure 3). One notable difference between ambient reflectance and emissivity is that the reflectance $RB_1$ is much sharper and narrower compared to the ambient emissivity $RB_1$ for pyroxene at all regolith porosities.

### 4.4. Transparency Features

The TF is a volume scattering feature whose position and depth (in emissivity) have been linked to particle size (Mustard & Hays, 1997). As particle size decreases to ~5 μm the TF shifts toward shorter wavelengths and deepens systematically (Mustard & Hays, 1997). Martin et al. (2022, 2023) found that the TF position does not change substantially with regolith porosity, while the depth of the TF increases as regolith porosity increases. In the ambient emissivity spectra presented here, the TF positions shift slightly toward longer wavelengths (Figure 4) and increase in spectral contrast as regolith porosity increases. Shirley and Glotch (2019) reported slightly higher TF spectral contrasts in their SAE spectra compared to ambient emissivity; However, they did not report spectral contrast values. As with the CF and RBs, the ambient emissivity TFs have positions and spectral contrasts similar to the TFs in reflectance spectra. The SAE spectra of both 0% regolith porosity 45–63 μm samples lack deep TFs (Figures 1 and 3). In fact, neither olivine SAE spectral suite develops an appreciable TF until ~50% regolith porosity. This is consistent with weak or absent TFs in high vacuum emissivity spectra reported by Logan and Hunt (1970) and Salisbury et al. (1991) attributed to thermal gradients. The formation of the TF with increasing regolith porosity indicates this feature is not only affected by particle size but also by

regolith porosity in reflectance and emissivity space. We find that the position of the TF in spectra of 0% regolith porosity olivine samples is dependent on environmental conditions (Tables 1 and 2). Conversely, the TF position in pyroxene and olivine (<20 μm) spectra with regolith porosity higher than 10% is independent of environmental conditions (Figure 4).

## 5. Discussion

### 5.1. Surface Versus Volume Scattering

In our previous work, we found that reflectance spectra of samples with low regolith porosity were characteristic of a regime where surface scattering dominated, whereas spectra of samples with high regolith porosity were characteristic of a regime where volume scattering dominated, with the transition between regimes being gradual (Martin et al., 2022, 2023). Emissivity spectra of olivine taken in ambient conditions follow a very similar scattering regime trend, yet the SAE spectra require a higher regolith porosity to transition into a volume scattering regime. For example, one indicator of samples transitioning from surface to volume scattering is that the spectral contrast of the CF decreases. While the CFs in SAE spectra reduce in spectral contrast as regolith porosity increases, it has a higher spectral contrast in high regolith porosity spectra compared to the ambient spectra for the olivine series (Figures 1 and 2). The higher spectral contrast in the SAE CFs in high regolith porosity spectra likely stems from a combination of effects in the SAE samples related to the thermal gradient in the top hundreds of microns. In SAE, photons associated with the CF are emitted from deeper in the sample (or regolith) and have a warmer temperature than the near surface photons.

The cause of the CF position disparity between SAE and ambient spectra is nuanced. Two explanations for the CF have been put forward in the literature: (a) $n$ (the real component of the complex index of refraction) passing through 1 leads into wavelengths of anomalous dispersion near a strong band, causing scattering off of particle boundaries to diminish (since $n$ is the same as the surrounding vacuum/air) and allowing photons to penetrate (or escape from) deeper in the surface (Conel, 1969; Salisbury et al., 1991). (b) Hapke (2012) points out, though, that the CF does not occur exactly where $n = 1$ and that a CF can also occur in materials where $n$ does not pass through 1. Instead, Hapke (2012) suggests that the CF corresponds to the transition from volume to surface scattering in a strong band. We posit that Hapke's fundamental explanation of the cause of the CF is correct, but that increased photon path length where $n = 1$ can also affect the SAE emissivity spectrum when steep thermal gradients are present. In this case, photons escaping from the hotter sub-surface could push the effective peak of the CF closer to $n = 1$. If true, we expect darker surfaces with minimal thermal gradients to produce spectra with smaller CF position offsets (Lucey et al., 2017; Shirley et al., 2023). Additional evidence comes from measurements of low albedo meteorites and lunar soils that show less CF shift between ambient and SAE conditions (Bramble et al., 2021b; Donaldson Hanna et al., 2017, 2021). A smaller thermal gradient may be why the slightly lower albedo pyroxene samples produce spectra with smaller CF position offsets compared to olivine. As such, the capability of SAE spectra to transition into the volume scattering regime is likely, but not solely, albedo dependent.

Another signifier of the transition into a primarily volume scattering regime is the presence of a 10-μm plateau feature. In previous works, we found that the spectral contrast of the 10-μm feature depends on regolith porosity (the higher the regolith porosity, the greater the spectral contrast; Martin et al., 2022, 2023), which is consistent with what we see in the ambient emissivity spectra for both olivine and pyroxene suites. However, the SAE spectra lack this 10-μm feature (with the possible exception of the <20 μm olivine 50% regolith porosity spectrum), supporting our previous observation that samples measured in SAE need a higher regolith porosity to transition to volume scattering regime. We suspect that SAE spectra will eventually show a 10-μm feature at higher regolith porosities (>80%). However, without lowering the albedo of our sample materials, we cannot measure regolith porosities greater than ∼50% of fine particulate olivine or 70% of pyroxene to test this theory. Future studies should look at laboratory samples with lower albedos to allow for higher regolith porosity SAE measurements, which in turn are better analogs for Solar System objects.

### 5.2. Comparisons to Other Laboratory Studies

Donaldson Hanna et al. (2012) found that the position of the olivine CF is shifted by ∼0.11 μm when comparing emissivity spectra measured in lunar versus ambient conditions. Similarly, Shirley and Glotch (2019) found the CF position shifts ∼ 0.14 and 0.18 μm for <32 μm and 32–63 μm olivine particles, respectively, when measured in

lunar and ambient conditions, and Bramble et al. (2021a) found the CF shifts ~0.13 and ~0.15 μm for <25 and 25–125 μm forsterite powders, respectively, when measured in SAE conditions. We note that lunar condition measurements are similar to the SAE measurements presented here, except for the brightness temperature (up to 400 K for lunar relevant measurements). We find slightly larger offsets in CF positions when comparing 0% regolith porosity SAE and ambient emissivity measurements (Table 2). These larger position offsets may be due to differences in how the sample is packed in the sample holder, slightly different viewing geometries, and/or different amounts of clinging fines. In general, the offset in position decreases with increasing regolith porosity (Figure 4), suggesting that increasing the void space in the sample lessens the offset of the CF position. In addition to incorporating KBr into a sample, regolith porosity can be affected by how tightly a sample is packed in a sample cup. If the packing state is the cause for differences in offset, and CF offsets are likely due to thermal gradients in SAE measurements, then it follows that the thermal gradient is dependent on how tight a sample is packed. Furthermore, the potential difference in packing between studies may indicate that the cause for the position offsets (a different thermal gradient within the top ~100 μm of the sample) becomes less important at high regolith porosities (50%). However, as we were unable to take SAE measurements of >50% regolith porosity olivine samples, this parameter space has yet to be explored.

The position offset of $RB_1$ measured in ambient emissivity and SAE of 0% regolith porosity spectra for both olivine (~0.12 and 0.25 μm) and the pyroxene samples (0.06 μm) are broadly consistent with measured offsets in a compositionally similar olivine (~0.23 μm) and pyroxene (~0.19 μm; Donaldson Hanna et al., 2021; Table 3). While it is possible that the differences in position offset are due to differences in particle size fraction, as we found different offset values in the two olivine spectral suites, Shirley and Glotch (2019) measured zero offset for several particle sizes. For spectra in the surface scattering regime, we find that the position offsets are generally smaller for RBs compared to CFs—indicating RB positions are better for comparing spectra taken in ambient and SAE conditions (consistent with results in Hamilton (2010), Shirley and Glotch (2019), Bramble et al. (2021a), and Donaldson Hanna et al. (2021)). In nearly all spectral suites, the RBs decrease in spectral contrast with increasing regolith porosity (Figures 5–7). The RB spectral contrast decrease is not as linear as the CF trend. Additionally, above ~60% regolith porosity, the spectral contrast of some RBs begins to increase (e.g., $RB_1$ and $RB_3$ in olivine (45–63 μm) reflectance spectra). This nonlinear trend, and slight increase in spectral contrast, is likely due to the complex transition from surface to volume scattering as regolith porosity increases.

Shirley and Glotch (2019) and Donaldson Hanna et al. (2021) found no position offset in the TF position when comparing ambient and SAE emissivity spectra. The position offset we find (see Tables 1 and 2) likely stems from the wide and shallow shape of the SAE TFs in our samples compared to the ambient measurements, which is more difficult to analyze compared to deep TFs in Shirley and Glotch (2019) and Donaldson Hanna et al. (2021). It is important to note that the TF position and spectral contrast are more dependent on environmental conditions than on measurement type (i.e., ambient reflectance and emissivity are more similar than ambient emissivity and SAE spectra).

### 5.3. Thermophysics and Heat Transfer

As previously stated, we consider KBr to be an *optical* proxy for regolith porosity as KBr is transparent in the MIR. Importantly, KBr particles are not *thermophysical* proxies for regolith porosity as they would transfer heat through grain-to-grain contacts (similar to the silicate grains) compared to heat transfer across void space for a porous medium. In vacuum, heat is transferred between regolith particles via conduction across contacts where particles touch and by radiation across the void spaces between particles. It follows that any thermal gradient in a regolith in vacuum is directly tied to particle size and regolith porosity (e.g., Gundlach & Blum, 2012; Henderson & Jakosky, 1994, 1997; Logan et al., 1973; Salisbury et al., 1994). The thermal conductivities of KBr, forsteritic olivine, and the pyroxene augite are 4.81, 4.96, and 4.05 W/mK, respectively, so the KBr particles behave thermally very similar to the silicate particles (Horai, 1971). In our experiments, particle size is controlled and varies, but regolith porosity from the heat transfer perspective does not significantly change (note Sample Cup Porosity in Table 1). In the future, more constrained experiments that better approximate the heat transfer in void spaces may be useful to better understand how the resulting thermal gradients additionally affect the MIR spectra (e.g., careful dust deposition as in Tinker et al., 2023). Such constrained experiments may also help to disentangle the thermophysical and optical properties of KBr.

### 5.4. Implications for Airless Bodies and Kirchhoff's Law

For both olivine sample series, the RB position offset between ambient emissivity and reflectance measurements of 0% regolith porosity samples is consistent with the position offset recorded in Lane et al. (2011) and Hamilton (2010) who took reflectance and emissivity spectra of synthetic and natural olivine (Table 2). Interestingly, the difference in position for some features (i.e., CF and $RB_1$) decreases with increasing regolith porosity, while other feature positions offsets do not change at all. The similarity between ambient emissivity and reflectance spectra suggests that measurements of fine particles in high regolith porosity samples taken in reflectance can be compared to remote sensing spectra of airless bodies by accounting for environmental spectral effects (e.g., the CF position). The same environmental considerations that need to be accounted for when taking emissivity measurements under ambient conditions should be applied to reflectance spectra (e.g., the position and spectral contrast of the CF). However, high regolith porosity samples show less feature position offset due to environmental conditions. As such, we recommend factoring in the relative intensities of the features (e.g., compare $RB_1$ and $RB_3$ to the CF as described in Section 3.3) to determine the overall regolith porosity before accounting for the environmental effects that change the position of diagnostic features.

We note that the CF is more pronounced in SAE spectra of 0% regolith porosity samples than with other measurement techniques, but the trend in decreasing spectral contrast with increasing regolith porosity is similar, although the rate at which the contrast decreases is slower in the SAE spectra. This implies that spectra of airless bodies that lack a CF must have even higher regolith porosities than previously suggested (Lowry et al., 2022; Martin & Emery, 2023).

Though Kirchhoff's Law is technically only valid in isothermal hemispherical reflectance, we have shown that it is appropriate to convert ambient reflectance measurements to emissivity (E = 1-R) for both surface and volume scattering regime dominated spectra. Measurements made in ambient conditions (both reflectance and emissivity) transition from surface to volume scattering in a very similar manner. In SAE, higher regolith porosities are required to see spectral features indicative of volume scattering due to effects stemming from environmental conditions.

Importantly, many of the differences between emissivity spectra taken in ambient and SAE conditions (e.g., CF position) are the same when comparing ambient reflectance spectra and SAE spectra. In ambient reflectance spectra, the CF will be at slightly longer wavelengths compared to a remote sensing spectrum (~0.35 and 0.2 μm for olivine and pyroxene, respectively; Tables 1–3), and the RBs will be at shorter wavelengths (~0.35, 0.09, and 0.15 μm for $RB_1$, $RB_2$, and $RB_3$ respectively in olivine spectra). For mineralogical identification of olivine, the positions of $RB_2$ and $RB_3$ should be used, as their positions are most consistent regardless of the measurement environment or particle size. For pyroxene reflectance spectra, the RB positions will be at slightly shorter wavelengths compared to SAE spectra (~0.24, 0.12, and 0.18 μm for $RB_1$, $RB_2$, and $RB_3$ respectively; Table 3). As with olivine, mineralogical identification of pyroxene should be performed using $RB_2$ and $RB_3$ because their positions are the most similar in reflectance and SAE spectra, and because the position offset at all measured regolith porosities is roughly the same (Figure 4).

## 6. Conclusions and Future Work

In this paper, we have shown that MIR reflectance spectra of high regolith porosity olivine and pyroxene samples taken under ambient conditions are analogous to emissivity spectra of the same samples taken under ambient conditions. These measurements serve as an empirical test to Kirchhoff's Law (E = 1-R), which is only strictly applicable to hemispherical reflectance spectra of samples in thermal equilibrium. Though the reflectance spectra presented here were taken with a diffuse reflectance accessory (not hemispherical reflectance), we have shown that fine-particulate samples of olivine and pyroxene at all regolith porosities can be interpreted equivalently to ambient emissivity spectra with some minor caveats (e.g., the pyroxene $RB_1$ is sharper in reflectance, and CFs tend to be wider in emissivity). As the relationship between ambient and SAE emissivity spectra is well known (e.g., Bates et al., 2021; Bramble et al., 2021a, 2021b; Donaldson Hanna et al., 2021, 2012; Shirley & Glotch, 2019), researchers can confidently utilize ambient reflectance spectra for studying airless bodies by considering known environmental spectral effects.

The transition from surface to volume scattering as regolith porosity increases can be seen in all sample suites but to a lesser extent in SAE spectra. Though SAE spectra show some signs of the transition (e.g., CF spectral contrast

reduction), the transition seems to require a higher regolith porosity to fully transition into the volume scattering regime. The reason SAE spectra do not fully transition into the volume scattering regime may be because of KBr being a poor *thermophysical* proxy for regolith porosity. As we were unable to take SAE measurements of olivine samples over 50% regolith porosity, and pyroxene samples over 70% regolith porosity, we cannot investigate a threshold regolith porosity for volume scattering to become dominant.

In the future, we hope to perform similar measurements with low-albedo, high-regolith-porosity samples, which are not only easier to heat and maintain thermal gradients (Bates et al., 2021; Bramble et al., 2021b; Donaldson Hanna et al., 2019, 2021) but also more applicable to a wider range of planetary surfaces.

## Data Availability Statement

Data used in this manuscript are available (Martin et al., 2024).

**Acknowledgments**
We acknowledge that this work was done in Northern Arizona, at the base of the San Francisco Peaks, on homelands sacred to Native Americans throughout the region. Additional work was done in Central Florida on the traditional land of the Ais, Apalachee, Calusa, Timucua, and Tocobago tribes—as well as the Seminole Tribe of Florida and the Miccosukee Tribe of Indians of Florida. We thank Michael Bramble and Timothy Glotch, whose reviews significantly improved this paper, as well as an anonymous reviewer. This work was supported by the National Aeronautics and Space Administration's Science Mission Directorate Research and Analysis SSW program NH19ZDA001N. This work was additionally supported under NASA Cooperative Agreement 80NSSC19M0214 to the Center for Lunar and Asteroid Surface Science.

## References

Bates, H. C., Donaldson Hanna, K. L., King, A. J., Bowles, N. E., & Russell, S. S. (2021). A spectral investigation of aqueously and thermally altered CM, CM-An, and CY chondrites under simulated asteroid conditions for comparison with OSIRIS- Rex and Hayabusa2 observations. *Journal of Geophysical Research: Planets*, *126*(7). https://doi.org/10.1029/2021JE006827

Bramble, M. S., Milliken, R. E., & Patterson III, W. R. (2021a). Thermal emission measurements of ordinary chondrite mineral analogs in a simulated asteroid environment: 1. Constituent mineral phases. *Icarus*, *369*, 114561. https://doi.org/10.1016/j.icarus.2021.114561

Bramble, M. S., Milliken, R. E., & Patterson III, W. R. (2021b). Thermal emission measurements of ordinary chondrite mineral analogs in a simulated asteroid environment: 2. Representative mineral mixtures. *Icarus*, *369*, 114251. https://doi.org/10.1016/j.icarus.2020.114251

Conel, J. E. (1969). Infrared emissivities of silicates: Experimental results and a cloudy atmosphere model of spectral emission from condensed particulate mediums. *Journal of Geophysical Research*, *74*(6), 1614–1634. https://doi.org/10.1029/jb074i006p01614

Donaldson Hanna, K. L., Bowles, N. E., Warren, T. J., Hamilton, V. E., Schrader, D. L., McCoy, T. J., et al. (2021). Spectral characterization of Bennu analogs using PASCALE: A new experimental set-up for simulating the near-surface conditions of airless bodies. *Journal of Geophysical Research: Planets*, *126*(2). https://doi.org/10.1029/2020JE006624

Donaldson Hanna, K. L., Greenhagen, B. T., Patterson, W. R., Pieters, C. M., Mustard, J. F., Bowles, N. E., et al. (2017). Effects of varying environmental conditions on emissivity spectra of bulk lunar soils: Application to Diviner thermal infrared observations of the Moon. *Icarus*, *283*, 326–342. https://doi.org/10.1016/j.icarus.2016.05.034

Donaldson Hanna, K. L., Schrader, D. L., Cloutis, E. A., Cody, G. D., King, A. J., McCoy, T. J., et al. (2019). Spectral characterization of analog samples in anticipation of OSIRIS-REx's arrival at Bennu: A blind test study. *Icarus*, *319*, 701–723. https://doi.org/10.1016/j.icarus.2018.10.018

Donaldson Hanna, K. L., Wyatt, M. B., Thomas, I. R., Bowles, N. E., Greenhagen, B. T., Maturilli, A., et al. (2012). Thermal infrared emissivity measurements under a simulated lunar environment: Application to the Diviner Lunar Radiometer Experiment. *Journal of Geophysical Research*, *117*(E12), E00H05. https://doi.org/10.1029/2011JE003862

Gundlach, B., & Blum, J. (2012). Outgassing of icy bodies in the Solar System – II: Heat transport in dry, porous surface dust layers. *Icarus*, *219*(2), 618–629. https://doi.org/10.1016/j.icarus.2012.03.013

Hamilton, V. E. (2000). Thermal infrared emission spectroscopy of the pyroxene mineral series. *Journal of Geophysical Research*, *105*(E4), 9701–9716. https://doi.org/10.1029/1999je001112

Hamilton, V. E. (2010). Thermal infrared (vibrational) spectroscopy of mg-fe olivines: A review and applications to determining the composition of planetary surfaces. *Geochemistry*, *70*(1), 7–33. https://doi.org/10.1016/j.chemer.2009.12.005

Hamilton, V. E., Christensen, P. R., Haplan, H. H., Haberle, C. W., Rogers, A. D., Glotch, T. D., et al. (2021). Evidence for limited compositional and particle size variation on asteroid (101955) Bennu from thermal infrared spectroscopy. *Astronomy and Astrophysics*, *650*, A120. https://doi.org/10.1051/00046361/202039728

Hapke, B. (1996). Applications of an energy transfer model to three problems in planetary regoliths: The solid-state greenhouse, thermal beaming, and emittance spectra. *Journal of Geophysical Research*, *101*(E7), 16–840. https://doi.org/10.1029/96je00918

Hapke, B. (2012). *Theory of reflectance and emittance spectroscopy* (2nd). Cambridge University Press.

Henderson, B. G., & Jakosky, B. M. (1994). Near-surface thermal gradients and their effects on mid-infrared emission spectra of planetary surfaces. *Journal of Geophysical Research*, *99*(E9), 19063–19073. https://doi.org/10.1029/94je01861

Henderson, B. G., & Jakosky, B. M. (1997). Near-surface thermal gradients and mid-IR emission spectra: A new model including scattering and application to real data. *Journal of Geophysical Research*, *102*(E3), 6567–6580. https://doi.org/10.1029/96je03781

Hergenrother, C. W., Barucci, M. A., Barnouin, O., Bierhaus, B., Binzel, R. P., Bottle, W. F., et al. (2014). The design reference asteroids for the OSIRIS-REx mission target (101955) Bennu. Preprint at https://arxiv.org/abs/1409.4704

Horai, K. (1971). Thermal conductivity of rock-forming minerals. *Journal of Geophysical Research*, *76*(5), 1278–1308. https://doi.org/10.1029/jb076i005p01278

Izawa, M. R. M., King, P. L., Vernazza, P., Berger, J. A., & McCutcheon, W. A. (2021). Salt – a critical material to consider when exploring the solar system. *Icarus*, *359*(114238), 114328. https://doi.org/10.1016/j.icarus.2021.114328

Kelley, M. S., Woodward, C. E., Gehrz, R. D., Reach, W. T., & Harker, D. E. (2017). Mid-infraed spectra of comet nuclei. *Icarus*, *284*, 344–358. https://doi.org/10.1016/j.icarus.2016.11.029

King, P. L., Izawa, M. R. M., Vernazza, P., McCutcheon, W. A., Berger, J. A., & Dunn, T. (2011). Salt — A critical material to consider when exploring the solar system. In *42nd lunar and planetary science conference* (p. 1985).

Kumari, N., Glotch, T. D., Shirley, K. A., Greenhagen, B. T., & Byron, B. D. (2024). Effects of space weathering on the Christiansen feature position of lunar surface materials. *Icarus*, *412*, 115976. https://doi.org/10.1016/j.icarus.2024.115976

Lane, M. D., Glotch, T. D., Dyar, M. D., Pieters, C. M., Klima, R., Hiroi, T., et al. (2011). Midinfrared spectroscopy of synthetic olivines: Thermal emission, specular and diffuse reflectance, and attenuated total reflectance studies of forsterite to fayalite. *Journal of Geophysical ResearchEducational Planning*, *116*(E8), E08010. https://doi.org/10.1029/2010JE003588

Logan, L. M., & Hunt, G. R. (1970). Emission spectra of particulate silicates under simu-lated lunar conditions. *Journal of Geophysical Research*, *75*(32), 6539–6548. https://doi.org/10.1029/jb075i032p06539

Logan, L. M., Hunt, G. R., Salisbury, J. W., & Balsamo, S. R. (1973). Compositional implications of Christansen frequency maximums for infrared remote sensing application. *Journal of Geophysical Research*, *78*(23), 4983–5003. https://doi.org/10.1029/jb078i023p04983

Lowry, V. C., Donaldson Hanna, K. L., Ito, G., Kelley, M. S. P., Campins, H., & Lindsay, S. (2022). T-Matrix and Hapke modeling of the thermal infrared spectra of Trojan asteroids and (944) Hidalgo: Implications for their regolith particle size and porosity. *The Planetary Science Journal*, *3*(14pp), 181. https://doi.org/10.3847/PSJ/ac7a30

Lucey, P. G., Greenhagen, B. T., Song, E., Arnold, J. A., Donaldson Hanna, K., Bowles, N. E., et al. (2017). Space weathering effects in Diviner Lunar Radiometer multispectral infrared measurements of the lunar Christiansen Feature: Characteristics and mitigation. *Icarus*, *283*, 343–351. https://doi.org/10.1016/j.icarus.2016.05.010

Martin, A. C., & Emery, J. P. (2023). MIR spectra and analysis of Jovian Trojan asteroids. *The Planetary Science Journal*, *4*(8), 153. https://doi.org/10.3847/PSJ/aced0c

Martin, A. C., Emery, J. P., & Loeffler, M. J. (2022). Spectral effects of regolith porosity in the mid-IR – Forsteritic olivine. *Icarus*, *378*, 114921. https://doi.org/10.1016/j.icarus.2022.114921

Martin, A. C., Emery, J. P., & Loeffler, M. J. (2023). Spectral effects of regolith porosity in the mid-IR – Pyroxene. *Icarus*, *397*, 115507. https://doi.org/10.1016/j.icarus.2023.115507

Martin, A. C., Emery, J. P., Loeffler, M. J., & Donaldson Hanna, K. L. (2024). Mid-infrared reflectance and emissivity spectra of high porosity regoliths [Dataset]. *Zenodo*. https://doi.org/10.5281/zenodo.13308246

Maturilli, A., Helbert, J., D'Amore, M., & Ferrari, S. (2015). Experimental verification of validity for Kirchhoff´S law (E=1-R) in vacuum and purged air. In *46th lunar and planetary science conference Houston TX* (p. 1722).

Maturilli, A., Helbert, J., Ferrari, S., Davidsson, B., & D'Amore, M. (2016). Characterization of asteroid analogues by means of emission and reflectance spectroscopy in the 1- to 100-μm spectral range. *Earth Planets and Space*, *68*(1), 113. https://doi.org/10.1186/s40623-016-0489-y

Mustard, J. F., & Hays, J. E. (1997). Effects of hyperfine particles on reflectance spectra from 0.3 to 25 mm. *Icarus*, *125*(1), 145–163. https://doi.org/10.1006/icar.1996.5583

Salisbury, J. W., D'Aria, D. M., & Jarosewich, E. (1991). Midinfrared (2.5–13.5 μm) reflectance spectra of powdered stony meteorites. *Icarus*, *92*(2), 280–297. https://doi.org/10.1016/0019-1035(91)90052-u

Salisbury, J. W., & Wald, A. (1992). The role of volume scattering in reducing spectral contrast of reststrahlen bands in spectra of powdered minerals. *Icarus*, *96*(1), 121–128. https://doi.org/10.1016/0019-1035(92)90009-v

Salisbury, J. W., Wald, A., & D'Aria, D. M. (1994). Thermal-infrared remote sensing and Kirchhoff's law 1. Laboratory measurements. *Journal of Geophysical Research*, *99*(B6), 11–911. https://doi.org/10.1029/93JB03600

Shirley, K. A., & Glotch, T. D. (2019). Particle size effects on mid-infrared spectra of lunar analog minerals in a simulated lunar environment. *Journal of Geophysical Research: Planets*, *124*(4), 970–988. https://doi.org/10.1029/2018JE005533

Shirley, K. A., Glotch, T. D., Donaldson, O., Trelewicz, J., Yang, Y., & Zhang, H. (2023). Effects of albedo on the MIR emissivity spectra of silicates for lunar comparison. *Journal of Geophysical Research: Planets*, *128*(4). https://doi.org/10.1029/2022JE007629

Takir, D., Emery, J. P., & McSween, H. Y. (2015). Toward an understanding of phyllosilicate mineralogy in the outer main asteroid belt. *Icarus*, *257*, 185–193. https://doi.org/10.1016/j.icarus.2015.04.042

Tinker, C. R., Glotch, T. D., Breitenfeld, L. B., Ryan, A., & Li, L. (2023). Experimental and analytical methods for thermal infrared spectroscopy of complex dust coatings in a simulated asteroid environment. *RAS Techniques and Instruments*, *2*(1), 723–734. https://doi.org/10.1093/rasti/rzad047

Vernazza, P., Delbo, M., King, P. L., Izawa, M. R. M., Olofsson, J., Lamy, P., et al. (2012). High surface porosity as the origin of emissivity features in asteroid spectra. *Icarus*, *221*(2), 1162–1172. https://doi.org/10.1016/j.icarus.2012.04.003

Williams, J. P., Paige, D. A., Greenhagen, B. T., & Sefton-Nash, E. (2017). The global surface temperatures of the Moon as measured by the Diviner Lunar Radiometer Experiment. *Icarus*, *283*, 300–325. https://doi.org/10.1016/j.icarus.2016.08.012

Young, C. L., Poston, M. J., Wray, J. J., Hand, K. P., & Carlson, R. W. (2019). The mid-IR spectral effects of darkening agents and porosity on the silicate surface features of airless bodies. *Icarus*, *321*, 71–81. https://doi.org/10.1016/j.icarus.2018.10.032